

# The nature of the two energy scales in underdoped superconducting cuprates

B. Valenzuela and E. Bascones

*Instituto de Ciencia de Materiales de Madrid, CSIC. Cantoblanco. E-28049 Madrid, Spain\**

(Dated: December 2, 2024)

Raman and ARPES experiments have demonstrated that in superconducting underdoped cuprates nodal and antinodal regions are characterized by two energy scales instead of the one expected in BCS. Using the Yang, Rice and Zhang (YRZ) model, in which pseudogap and superconductivity compete below a critical doping, we explain the deviations from BCS. We find that the antinodal Raman pair-breaking peak shifts to higher frequency with underdoping, follows the antinodal ARPES gap and is closely connected with the pseudogap. Its intensity decreases due to the competition between pseudogap and superconductivity. The nodal scale follows the doping dependence of the superconducting order parameter.

The pseudogap (PG) state of underdoped (UD) cuprates is characterized by a nodal-antinodal dichotomy with Fermi arcs at the diagonals of the Brillouin zone (BZ) (nodal region) and a gapped antinodal region<sup>1,2</sup>. On spite of several experimental claims of deviations from BCS<sup>3,4,5,6</sup>, it is generally believed that the superconducting (SC) state is standard<sup>7</sup>. Recently, Raman experiments<sup>8</sup> have confirmed the dichotomy in the SC state.

Inelastic Raman scattering probes the zero-momentum charge excitations. The response of nodal ( $\chi_{B_{2g}}$ ) and antinodal regions ( $\chi_{B_{1g}}$ ) can be separated. In the SC state pair-breaking peaks appear in the spectra. As the normal state of cuprates is characterized by a not yet understood broad continuum, these peaks are better identified in the subtracted response in SC and normal states  $\Delta\chi_{B_{1g,2g}} = \chi_{B_{1g,2g}}^{SC} - \chi_{B_{1g,2g}}^N$ . With a standard d-wave BCS gap  $\Delta_S \cos(2\phi)$ , the frequency and intensity of these peaks in both  $B_{2g}$  and  $B_{1g}$  channels are controlled by  $\Delta_S$ .

Opposite to BCS behavior, the experiments<sup>8</sup> reveal that in UD cuprates  $\Delta\chi_{B_{1g}}$  and  $\Delta\chi_{B_{2g}}$  show pair breaking peaks with opposite evolution with doping. The  $B_{1g}$  peak shifts to higher energy and loses intensity with underdoping, while the  $B_{2g}$  peak shifts to lower frequency without too much change in intensity. The Raman spectrum, specially the intensity of the  $B_{1g}$  peak has been one of the experimental results more difficult to understand. A BCS gap with higher harmonics<sup>8</sup>, and vertex corrections<sup>9</sup> or a very strongly anisotropic renormalization of the quasiparticle<sup>8</sup> have been invoked to explain the  $B_{1g}$  peak frequency and intensity, respectively.

Previously ARPES measurements<sup>3</sup> uncovered that underdoping leads to an increase in the gap in the antinodal region  $\Delta_{max}$  and a decrease in the slope of the gap at the nodes,  $v_\Delta$ , resulting in a U-shape dependence of the gap<sup>3,4</sup> instead of the V-shape expected from d-wave BCS. In the standard d-wave model,  $\Delta_S$  gives both  $v_\Delta$  and  $\Delta_{max}$ . A single-energy scale and a linear (V-shape) dependence on  $\cos(2\phi)$  of the gap are observed in the ARPES and Raman spectrum of overdoped cuprates<sup>2,6</sup>.

We propose a natural way to understand the nodal and antinodal energy scales in Raman and ARPES experiments within a model in which superconductivity and PG compete. We use the ansatz proposed by Yang, Rice

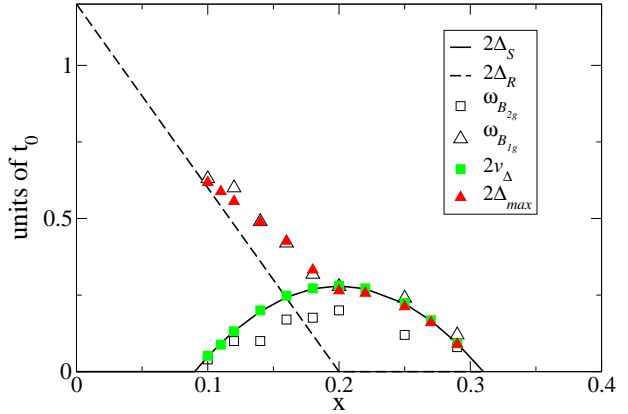


FIG. 1: (Color online) Comparison of pseudogap  $\Delta_R$  and superconducting  $\Delta_S$  scales with ARPES (filled symbols) and Raman energy scales (empty symbols). The YRZ parameters used depend on doping as,  $\Delta_R(x)/2 = 0.3(1 - x/0.2)$ ,  $\Delta_S(x)/2 = 0.07(1 - 82.6(x - 0.2)^2)$ ,  $t(x) = g_t(x) + 0.169/(1 + x)^2$ ,  $|t'(x)| = g_t(x)|t'_0|$  with  $t'_0 = -0.3$ ,  $t''(x) = g_t(x)t''_0$  with  $t''_0 = 0.2$  in units of the bare hopping  $t_0$ .

and Zhang<sup>10</sup> for the PG. The SC order parameter and the strength of the PG are respectively given by  $\Delta_S$  and  $\Delta_R$ . The later vanishes at a topological quantum critical point (QCP). Fig. 1 and the evolution of the Raman intensity with doping  $x$  are our main results. Only the nodal energy scale follows the non-monotonic dependence of the SC order parameter, being the slope of the gap at the nodes  $v_\Delta$  a good measure of  $\Delta_S$ . The antinodal energy scale, i.e. the location of the  $B_{1g}$  Raman peak  $\omega_{B_{1g}}$  and the maximum gap  $\Delta_{max}$  in ARPES, is intimately connected with the PG. The Raman spectra is calculated at the bubble level, without vertex corrections. The decrease of intensity in the  $B_{1g}$  channel with underdoping is due to the competition of PG and superconductivity in the antinodal region. The renormalization of the quasiparticle weight  $g_t$  just enhances this effect.

The YRZ model assumes that the PG can be described as a doped spin liquid and proposes a phenomenological Green's function to characterize it.

$$G^{YRZ}(\mathbf{k}, \omega) = \frac{g_t}{\omega - \xi_{\mathbf{k}} - \Sigma_R(\mathbf{k}, \omega)} + G_{inc}. \quad (1)$$

Here  $\xi_{\mathbf{k}} = \epsilon_{0\mathbf{k}} - 4t'(x) \cos k_x \cos k_y - 2t''(x)(\cos 2k_x + \cos 2k_y) - \mu_p$ ,  $\epsilon_{0\mathbf{k}} = -2t(x)(\cos k_x + \cos k_y)$  and  $\mu_p$  is determined from the Luttinger sum rule.  $\Sigma_R(\mathbf{k}, \omega) = \Delta_R(\mathbf{k})^2/(\omega + \epsilon_{0\mathbf{k}})$  diverges at zero frequency at the umklapp surface  $\epsilon_{0\mathbf{k}}$ , and  $\Delta_R(\mathbf{k}) = \Delta_R(x)/2(\cos k_x - \cos k_y)$ . The coherent part is similar to the BCS diagonal Green's function with the non-trivial difference that in BCS, the self-energy diverges at the Fermi surface (FS) and not at the umklapp one. Besides there is no off-diagonal component of the Green's function in our case and  $\Delta_R$  does not break any symmetry. For finite  $\Delta_R$  the quasiparticle peak is split into two and the FS consists of hole pockets close to  $(\pm\pi/2, \pm\pi/2)$ . At  $x_c$ ,  $\Delta_R(x)$  vanishes at a topological transition and a complete FS is recovered. Following predictions of mean field theory<sup>11</sup> the coherent spectral weight factor,  $g_t = 2x/(1+x)$ , decreases with underdoping and vanishes at half filling. We use the same parameters proposed in the original paper<sup>10</sup> measured in units of the bare hopping  $t_0$ . Their dependence on doping is given in Fig. 1<sup>10</sup>.

Superconductivity is introduced in the standard way<sup>12</sup> as in Ref.<sup>10</sup>. The diagonal Green's function becomes

$$G_{SC}^{RVB}(\mathbf{k}, \omega) = \frac{g_t}{\omega - \xi_{\mathbf{k}} - \Sigma_R(\mathbf{k}, \omega) - \Sigma_S(\mathbf{k}, \omega)}. \quad (2)$$

$\Sigma_S(\mathbf{k}, \omega) = |\Delta_S^2(\mathbf{k})|/(\omega + \xi(\mathbf{k}) + \Sigma_R(\mathbf{k}, -\omega))$  is the SC self energy with  $\Delta_S(\mathbf{k}) = \Delta_S(x)/2(\cos k_x - \cos k_y)$  with doping dependence given in Fig. 1. Each quasiparticle peak splits into four with energies  $\pm E_{\pm}$ .

$$\begin{aligned} (E_{\mathbf{k}}^{\pm})^2 &= \Delta_{R\mathbf{k}}^2 + \frac{\xi_{\mathbf{k}}^2 + \xi_{0\mathbf{k}}^2 + \Delta_{S\mathbf{k}}^2}{2} \pm (E_{\mathbf{k}}^{SC})^2 \\ (E_{\mathbf{k}}^{SC})^2 &= \sqrt{(\xi_{\mathbf{k}}^2 - \xi_{0\mathbf{k}}^2 + \Delta_{S\mathbf{k}}^2)^2 + 4\Delta_{R\mathbf{k}}^2((\xi_{\mathbf{k}} - \xi_{0\mathbf{k}})^2 + \Delta_{S\mathbf{k}}^2)} \end{aligned}$$

The spectral functions  $A(\mathbf{k}, \omega) = -2\text{Im}G(\mathbf{k}, \omega)$  and  $B(\mathbf{k}, \omega) = -2\text{Im}F(\mathbf{k}, \omega)$  with  $F(\mathbf{k}, \omega)$  the anomalous Green's function are

$$\begin{aligned} A(\mathbf{k}, \omega) &= g_t \pi \{ (v_{\mathbf{k}}^-)^2 \delta(\omega + E_{\mathbf{k}}^-) + (u_{\mathbf{k}}^-)^2 \delta(\omega - E_{\mathbf{k}}^-) \\ &\quad + (v_{\mathbf{k}}^+)^2 \delta(\omega + E_{\mathbf{k}}^+) + (u_{\mathbf{k}}^+)^2 \delta(\omega - E_{\mathbf{k}}^+) \}, \\ B(\mathbf{k}, \omega) &= g_t \pi \{ u_{\mathbf{k}}^- v_{\mathbf{k}}^- (\delta(\omega + E_{\mathbf{k}}^-) + \delta(\omega - E_{\mathbf{k}}^-)) \\ &\quad + u_{\mathbf{k}}^+ v_{\mathbf{k}}^+ (\delta(\omega + E_{\mathbf{k}}^+) + \delta(\omega - E_{\mathbf{k}}^+)) \}, \end{aligned} \quad (3)$$

with coherence factors  $v_{\mathbf{k}}^{2\pm} = \frac{1}{2}(a_{\mathbf{k}}^{\pm} - b_{\mathbf{k}}^{\pm}/E_{\mathbf{k}}^{\pm})$  and  $u_{\mathbf{k}}^{2\pm} = \frac{1}{2}(a_{\mathbf{k}}^{\pm} + b_{\mathbf{k}}^{\pm}/E_{\mathbf{k}}^{\pm})$ , where  $a_{\mathbf{k}}^{\pm} = \frac{1}{2}(1 \pm (\xi_{\mathbf{k}}^2 - \xi_{0\mathbf{k}}^2 + \Delta_{S\mathbf{k}}^2)/E_{\mathbf{k}}^{SC})$  and  $b_{\mathbf{k}}^{\pm} = \xi_{\mathbf{k}} a_{\mathbf{k}}^{\pm} \pm \Delta_{R\mathbf{k}}^2(\xi_{\mathbf{k}} - \xi_{0\mathbf{k}})$ .

In the bubble approximation<sup>13</sup> the Raman response is

$$\text{Im}\{\chi_{\gamma\nu}(\Omega)\} = \sum_{\mathbf{k}} (\gamma_{\mathbf{k}}^{\nu})^2 \int \frac{d\omega}{4\pi} (n_F(\omega) - n_F(\omega + \Omega)) \{ A(\mathbf{k}, \omega + \Omega) A(\mathbf{k}, \omega) - B(\mathbf{k}, \omega + \Omega) B(\mathbf{k}, \omega) \}. \quad (4)$$

Here  $n_F(\omega)$  is the Fermi function,  $\nu = B_{1g}, B_{2g}$  and  $\gamma_{\mathbf{k}}^{\nu}$ , the  $B_{1g}$  and  $B_{2g}$  Raman vertices, are proportional to  $\cos k_x - \cos k_y$  and  $\sin k_x \sin k_y$  respectively.

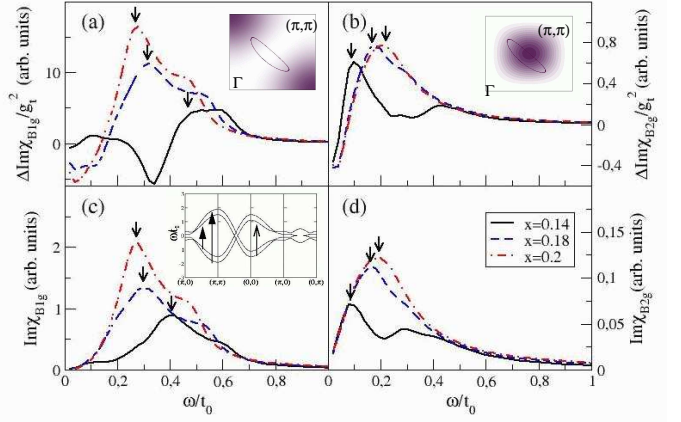


FIG. 2: Insets in (a) and (b): Raman vertices  $(\gamma_{\mathbf{k}}^{B_{1g}})^2$  and  $(\gamma_{\mathbf{k}}^{B_{2g}})^2$  in the first quadrant of the BZ, with the Fermi pocket for  $x = 0.14$  drawn. Inset in (c): bands for  $x = 0.14$  in the SC state. The arrows signal the possible optical transitions. Main figures (a) and (b) subtracted Raman response in  $B_{1g}$  and  $B_{2g}$  polarizations divided by the coherent weight factor  $g_t^2$ , for  $x = 0.14$  and  $x = 0.18$  in the underdoped regime and to  $x_c = 0.20$ . (c) and (d) full Raman response in the  $B_{1g}$  and  $B_{2g}$  channels respectively for the same dopings. Raman units are the same for all dopings. The arrows indicate the position,  $\omega_{B_{1g}}$  and  $\omega_{B_{2g}}$ , and intensity of the pair breaking peaks. The  $\delta$  functions in Eq. 3 have been replaced by Lorenzians with a width of  $0.05t(x)$  with  $t(x)$  given in Fig. 2a.

The dependence on  $x$  of the nodal and antinodal subtracted Raman spectra  $\Delta\chi$  can be seen in Fig. 2a and 2b. Two different energy scales  $\omega_{B_{1g}}$  and  $\omega_{B_{2g}}$  appear for finite  $\Delta_R$ . These scales, signalled by an arrow in Fig. 2, are plotted in Fig. 1. At  $x_c = 0.2$  the PG vanishes and  $\Delta\chi_{B_{1g}}$  and  $\Delta\chi_{B_{2g}}$  peaks appear at an energy close to  $2\Delta_S$ . This is the expected behavior for a BCS superconductor<sup>14</sup>. On the contrary, as  $x$  is reduced the  $\Delta\chi_{B_{1g}}$  peak shifts to larger frequency and its intensity decreases, while the  $\Delta\chi_{B_{2g}}$  peak shifts to lower frequency with a weakly  $x$ -dependent intensity. This behavior resembles very much the experimental one<sup>8</sup>. In Fig. 2a and 2b the spectra have been divided by  $g_t^2$  to emphasize that the suppression of the intensity in the  $B_{1g}$  channel with underdoping is not only due to the reduction of the coherent part, as proposed in<sup>8</sup>. With  $g_t^2$  included the weakening of the  $B_{1g}$  transition with underdoping is enhanced and the  $B_{2g}$  signal decreases.

The appearance of two different energy scales for  $B_{1g}$  and  $B_{2g}$  response is associated to the two pair-breaking transitions in the inset of Fig. 2c with energies  $2E_{\pm}(\mathbf{k})$ . The distinction between nodal and antinodal signal has its origin in the coherence factors  $u_{\pm}^2(\mathbf{k})v_{\pm}^2(\mathbf{k})$  which weight each transition. Shown in Fig. 3a (Fig. 3b) for  $x = 0.14$ ,  $u_{-}^2(\mathbf{k})v_{-}^2(\mathbf{k})$  ( $u_{+}^2(\mathbf{k})v_{+}^2(\mathbf{k})$ ), weights more heavily the nodal (antinodal) region. The  $B_{2g}$  and  $B_{1g}$  spectra are respectively dominated by the transitions with energy  $2E_{-}$  and  $2E_{+}$ . The maxima in the Raman spec-

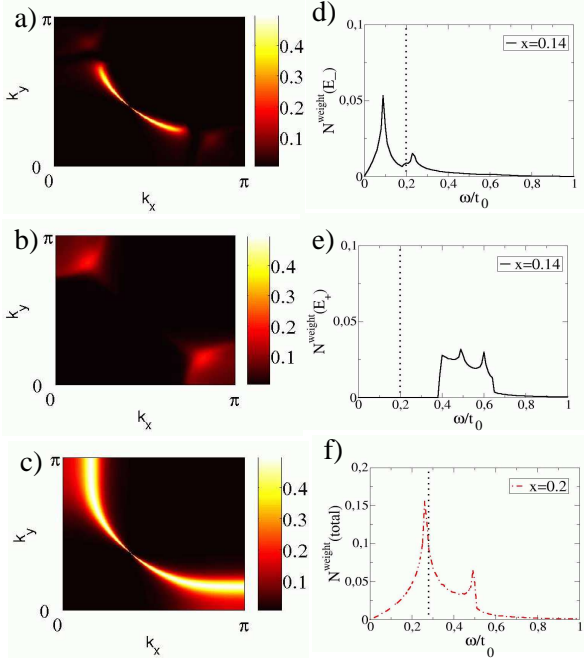


FIG. 3: (a) to (c) coherence factors, in the first quadrant of the BZ, corresponding to the pair breaking transitions with energies  $2E_{\pm}$  (see text). The weighted densities of transitions  $N_{weight}(E_{\pm})$  are plotted in (d) to (f).  $2\Delta_S$  is marked with a dotted line. The added coherence factors and total weighted density of transitions for  $x_c = 0.2$  (critical doping) are shown in (c) and (e) recovering the d-wave BCS result.

tra in Fig. 2a and 2b arise from the peaks in the densities of transitions  $N_{2E_{\pm}}^{weight} = \sum_{\mathbf{k}} u_{\pm}^2(\mathbf{k}) v_{\pm}^2(\mathbf{k}) \delta(\omega - 2E_{\pm}(\mathbf{k}))$ . In Fig. 3d  $N_{2E_{-}}^{weight}$  peaks at a frequency smaller than  $2\Delta_S$ .  $\omega_{B_{2g}}$  depends not only on  $\Delta_S$  but also on the length of the Fermi pockets along  $(\pi, 0)$ - $(0, \pi)$  as its value comes from the edges of the Fermi pockets. Due to the shrinking of the pockets with increasing  $\Delta_R$ ,  $\omega_{B_{2g}}$  is shifted to lower frequencies with underdoping, even if a doping independent  $\Delta_S$  is used. In Fig. 3e, the energy at which  $N_{2E_{+}}^{weight}$  peaks is determined by a saddle-point close to  $(\pi, 0)$ , along  $(\pi, 0) - (\pi, \pi)$  and is bigger than  $2\Delta_S$ . In the UD region, this energy is mainly controlled by  $\Delta_R$ . If  $x \geq x_c$ , only one of the pair-breaking transitions gives a finite contribution for a given  $\mathbf{k}$ . A complete d-wave superconducting gap is recovered and, as shown in Fig. 3c it is tracked by the added coherence factors  $u_{+}^2(\mathbf{k}) v_{+}^2(\mathbf{k}) + u_{-}^2(\mathbf{k}) v_{-}^2(\mathbf{k})$ . The maximum in  $N_{E_{-}}^{weight}$  is not anymore a maximum of the total density of weighted transitions  $N_{tot}^{weight} = N_{E_{-}}^{weight} + N_{E_{+}}^{weight}$ , plotted in Fig. 3f, but both densities of transitions match perfectly.  $N_{tot}^{weight}$  is now the meaningful quantity and it peaks close to  $2\Delta_S$  recovering the BCS result with a single energy scale<sup>14</sup>.

A third *crossing* transition, with energy  $E_{-}(\mathbf{k}) + E_{+}(\mathbf{k})$ , and larger intensity in the  $B_{1g}$  channel is also

allowed if  $\Delta_R$  is finite, as shown in the inset of Fig. 2c. Its effect is small in  $\Delta\chi$ , as it is expected in both the PG and the SC state. The total responses  $\chi_{B_{1g}}^{SC}$  and  $\chi_{B_{2g}}^{SC}$  including the contribution of this crossing transition in the SC state are plotted in Figs. 3c and 3d. It is not easy to distinguish this transition from the pair-breaking ones. To the best of our knowledge this transition has not been found yet in the PG state but it could be hidden in the broad background due to strong inelastic scattering.

As expected for a gap with nodes, the  $B_{2g}$  response in Fig. 3d is linear at low frequencies. The slope is doping independent. This independence, observed also experimentally<sup>8</sup>, comes from a cancellation between the dependencies of the quasiparticle weight squared  $g_t^2$ , the SC order parameter,  $\Delta_S$ , and the density of states, via the renormalization of the band parameters.

The nodal and antinodal scales can be also seen in ARPES. For  $x < x_c$  in the PG state, the FS consists of closed hole pockets. However, due to the weak spectral weight of the quasiparticle pole in the outer edge of the pocket, the ARPES spectra resembles the Fermi arcs observed experimentally. The length of these arcs increases with doping, as seen in Fig. 4a and Fig. 4b. A complete FS is recovered when  $\Delta_R = 0$  in Fig. 4c. In the absence of a complete FS, to analyze the  $\mathbf{k}$ -dependence of the gap we take the surface with maximal intensity  $\omega = 0$  and  $\Delta_S = 0$ . This surface, signalled in blue in the pictures, resembles the one interpreted experimentally as the underlying FS. To compare with experiments<sup>3</sup> we define  $v_{\Delta}$  as the derivative of the energy with respect to  $\cos k_x - \cos k_y$  at the nodes<sup>15</sup> and  $\Delta_{max}$  as the maximum gap along this surface. Shown in Fig. 4d for  $x = 0.05$ , when  $\Delta_S$  is zero but  $\Delta_R$  finite, the energy vanishes along the arc and a gap opens linearly with  $\cos k_x - \cos k_y$  from the arc edge.  $\Delta_{max}$  increases with underdoping. A finite  $\Delta_S$  opens a gap along the arc in Fig. 4e. This gap depends linearly on  $\cos k_x - \cos k_y$ , with slope  $v_{\Delta}$  very close to  $\Delta_S$ . Outside the arc, the gap depends on both  $\Delta_R$  and  $\Delta_S$ . In this UD SC region  $v_{\Delta}$  increases with doping and  $\Delta_{max}$  decreases (see Fig. 1). Correspondingly, the spectra does not depend linearly on  $\cos k_x - \cos k_y$  but has a U-shape dependence on  $\cos k_x - \cos k_y$  with a kink around the arc edge. Deviations from linearity increase with underdoping. In Fig. 4f, at  $x = x_c$ , the linear V-shape BCS dependence re-appears and  $v_{\Delta}$  and  $\Delta_{max}$  converge.

The evolution of ARPES scales  $v_{\Delta}$  and  $\Delta_{max}$ , with doping is plotted in Fig. 1, and compared with the ones found in Raman and the input  $\Delta_S$  and  $\Delta_R$ . The similarity with experimental data is striking<sup>8</sup>. With the  $\Delta_S(x)$  used,  $\omega_{B_{2g}}$  and  $v_{\Delta}$  are non-monotonic on doping. On the other hand, the frequency at which  $B_{1g}$  peaks  $\omega_{B_{1g}}$  follows very closely  $2\Delta_{max}$  and both decrease as  $\Delta_R$  does. Twice the gap value at  $(\pi, 0)$ , sometimes compared in the literature with  $\omega_{B_{1g}}$ , is expected to be a bit larger than  $2\Delta_{max}$  plotted here. The nodal and antinodal scales merge when the pseudogap correlations disappear.

In conclusion, we have explained the deviations from BCS in Raman and ARPES experiments in underdoped

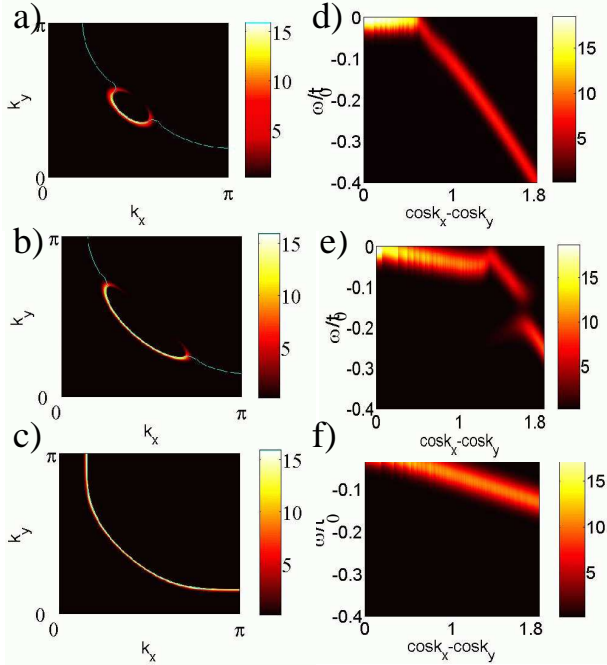


FIG. 4: (a) to (c) Map of ARPES intensity in the first quadrant of the BZ, at zero frequency and zero  $\Delta_S$  for (a)  $x = 0.05$ , (b)  $x = 0.14$  and (c)  $x_c = 0.20$ . In blue, the maximum intensity surface. (d) to (f) Energy spectrum corresponding to (d)  $x=0.05$ , (e)  $x=0.14$  and (f)  $x=0.20$ , along the surface marked in (a) to (c).  $\Delta_S$  is finite in (e) and (f). The  $\delta$  functions in  $A(\mathbf{k}, \omega)$ , have been replaced by lorenzians of width  $0.001t_0$  and the spectral function convoluted with a gaussian of width  $0.02t_0$  ( $\sim 6 - 10$  meV) and a temperature  $T = 0.001t_0$ .

superconducting cuprates. Nodal and antinodal energy scales which evolve in opposite manner with doping appear in both spectra. The  $B_{2g}$  response, that reflects the transitions in the nodal region, peaks at a frequency  $\omega_{B_{2g}}$  which qualitatively follows the doping dependence of the superconducting order parameter  $\Delta_S$ . On the contrary, the energy of the pair breaking transitions in the antinodal region,  $\omega_{B_{1g}}$ , decreases monotonically with increasing doping and its intensity decreases with underdoping due to the competition between pseudogap and

superconducting correlations. This nodal-antinodal dichotomy can be explained in terms of two different pair-breaking transitions which selectively weight the nodal and antinodal region. Twice the maximum value of the gap  $\Delta_{max}$  along the maximum intensity surface follows very closely  $\omega_{B_{1g}}$ . Within this model the slope of the gap at the nodes,  $v_\Delta$ , as measured by ARPES, is a good measure of  $\Delta_S$  while the maximum value of the gap  $\Delta_{max}$  arises from an interplay between the pseudogap  $\Delta_R$  and  $\Delta_S$ . We emphasize that we have not tried to fit the experiments but just taken the values proposed in the YRZ paper<sup>10</sup>. For the values used,  $x_c$  and optimal doping coincide, but this might not be the case<sup>16</sup>.  $x_c$ , and not the doping with maximum  $\Delta_S$ , controls the appearance of anomalous behavior.

Similar two-scale behavior could appear in other models with a QCP<sup>17</sup>. Possible differences could be the decreasing spectral weight with underdoping, important for the constancy of the slope in  $B_{2g}$  channel, and the suppression of intensity<sup>18</sup>, seen in Fig. 4e which a priori are not expected in other QCP models. In the YRZ ansatz the FS is truncated without breaking of symmetry and a topological transition happens at  $x_c$ , in agreement with experiments<sup>16</sup> and Dynamical Mean Field Theory<sup>19</sup>. It is hard to understand a peak in  $\Delta\chi_{B_{1g}}$  in models with separation in  $\mathbf{k}$ -space in which antinodal quasiparticles, responsible of the pseudogap, do not participate in superconductivity<sup>20</sup>. While not included here, we believe that the appearance of two energy scales in the SC state is robust enough to survive inelastic scattering.

## Acknowledgments

We thank M. Le Tacon, A. Sacuto, L. Tassini, R. Hackl, J. Carbotte and G. Kotliar for discussions and M.A.H Vozmediano, A.V. Chubukov, F. Guinea and T.M. Rice for discussions and reading of the preprint. Funding from MCyT through MAT2002-0495-C02-01, FIS2005-05478-C02-01 and Ramon y Cajal and from Consejería de Educacion de la Comunidad de Madrid and CSIC through 200550M136 and I3P is acknowledged.

\* Electronic address: leni@icmm.csic.es, belen@icmm.csic.es

<sup>1</sup> T. Timusk and B. W. Statt, Rep. Prog. Phys. **62**, 61 (1999); M. R. Norman, D. Pines, and C. Kallin, Adv. Phys. **54**, 715 (2005).

<sup>2</sup> A. Damascelli, Z. Hussain, and Z-X. Shen, Rev. Mod. Phys. **75**, 473 (2003).

<sup>3</sup> J. Mesot *et al* Phys. Rev. Lett. **83**, 840 (1999).

<sup>4</sup> S. V. Borisenko, *et al* Phys. Rev. B **66**, 140509 (2002).

<sup>5</sup> C. Panagopoulos and T. Xiang, Phys. Rev. Lett. **81**, 2336 (1998).

<sup>6</sup> T. P. Devereaux, and R. Hackl, Rev. Mod. Phys. in press.

<sup>7</sup> J. Zaanen, *et al.*, Nature Physics **2**, 138 (2006).

<sup>8</sup> M. Le Tacon *et al*, Nature Physics **2**, 537 (2006).

<sup>9</sup> R. Zeyher and A. Greco, Phys. Rev. Lett. **89**, 177004 (2002); Y. Gallais *et al*, Phys. Rev. B **71**, 012506 (2005); A.V. Chubukov, T.P. Devereaux and M.V. Klein, Phys. Rev. B **73**, 094512 (2006).

<sup>10</sup> K-Y. Yang, T. M. Rice, and F-C Zhang, Phys. Rev. B **73**, 174501 (2006).

<sup>11</sup> F. C. Zhang, C. Gros, T. M. Rice, and H. Shiba, Supercond. Sci. Technol. **1**, 36-46 (1988).

<sup>12</sup> A. A. Abrikosov, L. P. Gor'kov, and I. E. Dzyaloshinskii,

*Methods of Quantum Field Theory in Statistical Physics*, (R.A. Silverman, revised edn. Dover, New York, (1975)).

<sup>13</sup> G. Mahan, *Many Particle Physics*, (Plenum Press, New York and London, 1990).

<sup>14</sup> In the continuum limit in a BCS superconductor the peak in  $\Delta\chi_{B_{1g}}$  appears exactly at  $2\Delta_S$ . In a lattice two peaks appear, the smaller peak at higher energy is given by band structure effects and ignored in the discussion.

<sup>15</sup>  $v_\Delta$  is normalized to  $\Delta_{max}$  for  $\Delta(\phi) = \Delta_{max}\cos(2\phi)^3$ .

<sup>16</sup> J. L. Tallon, and J. W. Loram, *Physica C* **349**, 53 (2001).

<sup>17</sup> S. Chakravarty, R. B. Laughlin, D. K. Morr, and C. Nayak, *Phys. Rev. B* **63**, 094503 (2001); C. M. Varma, *Phys. Rev. Lett* **83**, 3538 (1999); L. Benfatto, S. Caprara, C. Di Castro, *Eur. Phys. J. B* **71**, 95 (2000).

<sup>18</sup> The suppression of the intensity for some  $\mathbf{k}$  in the SC state is due to the mixing between the  $\pm E_\pm$  bands.

<sup>19</sup> T. D. Stanescu and G. Kotliar, *Phys. Rev. B* **74**, 125110 (2006).

<sup>20</sup> D. Pines, [cond-mat/0404151](https://arxiv.org/abs/cond-mat/0404151) (preprint).